

CHAPTER ONE HUNDRED SEVENTEEN

NUMERICAL SIMULATION ON THE CHANGE OF BOTTOM TOPOGRAPHY

BY THE PRESENCE OF COASTAL STRUCTURES

by

Masataka Yamaguchi¹ and Yōichi Nishioka²

ABSTRACT

This paper presents a numerical model for predicting the change of bottom topography caused by coastal structures placed on a sandy beach. The model consists of three sub-models of wave transformation by varying topography and coastal structures, nearshore current and change of bottom topography. The computation of nearshore current patterns induced by the presence of a detached breakwater shows qualitative agreement with the experiment. The effects of wave and structure characteristics on current pattern and topographical change are investigated by consideration of model computation with several configurations of coastal structures such as detached breakwaters or groins. The main conclusions are that the model produces the general features of erosion and deposition caused by coastal structures and that drastic change of current pattern and bottom topography occur when reflected waves from the structures cover a large area.

1. INTRODUCTION

In recent years, shoreline models for predicting the changes in the plane shape of beach following the construction of coastal structures have been extensively used for practical applications. But, there are many limitations such that they neglect onshore-offshore sediment transport and assume parallel movement of the beach profile. In order to solve these problems, a more rational model, in which the effect of waves and nearshore currents in surf zone on sediment transport is explicitly included, is required. At the present stage of study, there are few works done from this point of view except for a numerical model by Fleming and Hunt (1976).

-
- 1) Prof., Dept. of Ocean Eng., Ehime Univ., Bunkyocho 3, Matsuyama 790, Ehime Pref., Japan
 - 2) Engineer, Ōsaka Prefectural Office, Ōtemaenomachi 2, Higashiku, Ōsaka 540, Ōsaka Pref., Japan

Their model may be useful for practical applications. But, the assumptions made in their model regarding nearshore current and so on seem to be too simplified.

A mathematical model to predict the topographical change caused by coastal structures was developed at our laboratory in 1981 and since then, much effort has been devoted to improving the model (1983a, 1983b and 1984). The model consists of three kinds of submodels of wave transformation by varying topography and coastal structures, wave-induced nearshore current and topographical change of the seabed. This paper presents the description of the latest model and the model computations of the characteristics of nearshore current patterns and bottom modifications caused by detached breakwaters or groins.

2. MODEL DESCRIPTION

(1) Wave transformation model

Wave transformation is computed by the wave ray method, in which the wave ray equation and wave intensity equation are solved simultaneously. The determination of wave direction along a ray is made by solving the wave ray equation expressed by time t ,

$$\frac{d\alpha}{dt} = \cos\alpha \frac{\partial c}{\partial x} - \sin\alpha \frac{\partial c}{\partial y} \quad (1)$$

in which α is the wave direction and c the wave celerity. The computation of wave refraction is made by the wave intensity equation,

$$\frac{d^2\beta}{dt^2} + p_t \frac{d\beta}{dt} + q_t \beta = 0, \quad \beta = K_r^{-2} \quad (2)$$

in which β is the ray separation factor, K_r the refraction factor, and p_t and q_t are the functions of α and the derivatives of c . The shoaling factor K_s is estimated by the well-known formula.

$$K_s^2 = c_{gM} / c_g \quad (3)$$

in which c_g is the group velocity and subscript 'M' means offshore wave characteristics.

In the model, bottom friction, diffraction, reflection and energy dissipation by wave breaking are approximately taken into account. But, wave-current interaction is not included. The Bretschneider-Reid formula on uniform depth is applied step by step to evaluate wave damping due to bottom friction. The diffraction effect of coastal structures is approximated by applying the Sommerfeld solution for semi-

infinite breakwater or its superposed solution to individual point on each wave ray. The Goda criterion (1975) is used to test whether wave breaking is occurring on each point along a wave ray or not. This is expressed as

$$\frac{H_b}{L_0} = 0.17 \left\{ 1 - \exp \left\{ -1.5 \frac{\pi D_b}{L_0} (1 + 15i^{4/3}) \right\} \right\} \quad (4)$$

in which H is the wave height, L the wave length, $D (=h+\eta)$ the total depth including wave set-up or wave set-down η , h the still water depth, i the bottom slope and subscripts '0' and 'b' mean deep water and wave breaking respectively. It is assumed that the waves break at a depth D if the wave height H is greater than H_b and that the wave height exceeding H_b does not exist in the surf zone.

The first step in the computation of wave transformation is to determine wave direction and wave height at each point along a wave ray and to cover the entire domain of interest with a great number of wave rays. Wave rays of not only incident waves but also diffracted waves from breakwater tip and reflected waves from structure wall are followed in succession.

The second step is to make linear interpolation of three kinds of wave data separately into each grid point prepared for the computation of nearshore current and topographical change, and to obtain single data of wave direction and wave height on each grid point through the energy composition of these data. Then, the radiation stress is estimated in the usual manner from the assumption of pure progressive waves.

(2) Nearshore current model

In order to compute nearshore current and wave set-up or set-down induced by waves, vertically integrated conservation of water mass and momentum are used. The conservation equation of water mass is given as

$$\frac{\partial D}{\partial t} + \frac{\partial DU}{\partial x} + \frac{\partial DV}{\partial y} = 0 \quad (5)$$

in which U and V are the nearshore current velocity components in x direction and in y direction respectively. The momentum equations are as follows.

$$\left. \begin{aligned} \frac{\partial DU}{\partial t} + \frac{\partial DU^2}{\partial x} + \frac{\partial DUV}{\partial y} &= -gD \frac{\partial \eta}{\partial x} \\ + \frac{1}{\rho} \left\{ \frac{\partial}{\partial x} (D\mu \frac{\partial U}{\partial x}) + \frac{\partial}{\partial y} (D\mu \frac{\partial U}{\partial y}) \right\} &- \frac{1}{\rho} \left(\frac{\partial S_{xx}}{\partial x} + \frac{\partial S_{xy}}{\partial y} + \tau_{bx} \right) \end{aligned} \right\} (6)$$

$$\left. \begin{aligned} \frac{\partial DV}{\partial t} + \frac{\partial DUV}{\partial x} + \frac{\partial DV^2}{\partial y} &= -gD \frac{\partial \eta}{\partial y} \\ + \frac{1}{\rho} \left\{ \frac{\partial}{\partial x} (D\mu_e \frac{\partial V}{\partial x}) + \frac{\partial}{\partial y} (D\mu_e \frac{\partial V}{\partial y}) \right\} - \frac{1}{\rho} \left(\frac{\partial S_{yx}}{\partial x} + \frac{\partial S_{yy}}{\partial y} + \tau_{by} \right) \end{aligned} \right\}$$

in which ρ is the density of fluid, μ_e the lateral mixing factor and S_{xx} , S_{xy} , S_{yx} and S_{yy} are the radiation stress tensor defined by Longuet-Higgins.

The Longuet-Higgins expression (1970) is used as lateral mixing factor.

$$\mu_e = \kappa \rho l \sqrt{gD} \tag{7}$$

in which l is the distance measured from the real shoreline and $\kappa(0.01)$ the constant. The bottom friction is assumed proportional to the squared velocity, taking into account the wave orbital velocity.

$$\left. \begin{aligned} \tau_b = (\tau_{bx}, \tau_{by}) &= \frac{\rho c_f}{T} \int_0^T |w| w dt \\ w &= (-u_{\max} \sin \alpha \cos \sigma t + U, -u_{\max} \cos \alpha \cos \sigma t + V) \\ u_{\max} &= \pi H / T \sinh kD \end{aligned} \right\} \tag{8}$$

in which c_f is the bottom friction coefficient in the wave-current system and σ the angular frequency. Eq. (8) is estimated by the Nishimura approximation formula (1982) to save the computation time without losing numerical accuracy. It can be written as

$$\left. \begin{aligned} \tau_{bx} &= \rho c_f \left\{ \left(w + \frac{\bar{u}^2}{w} \cos^2 \theta \right) U + \frac{\bar{u}^2}{w} \sin \theta \cos \theta V \right\} \\ \tau_{by} &= \rho c_f \left\{ \frac{\bar{u}^2}{w} \sin \theta \cos \theta U + \left(w + \frac{\bar{u}^2}{w} \sin^2 \theta \right) V \right\} \\ w &= \left(\sqrt{U^2 + V^2 + \bar{u}^2 + 2W\bar{u}} + \sqrt{U^2 + V^2 + \bar{u}^2 - 2W\bar{u}} \right) / 2 \\ W &= U \cos \theta + V \sin \theta, \quad \bar{u} = 2u_{\max} / \pi \end{aligned} \right\} \tag{9}$$

This formula approximates eq. (8) with high accuracy, as far as the wave orbital velocity of the small amplitude wave theory is used.

A finite difference model has been established to solve these equations. Fig. 1 is the coordinate system used in the nearshore current and topographical change computation, in which x axis and y axis are taken in the offshore direction and in the longshore direction respectively. Fig. 2 shows the configuration of variables in the finite difference model. Velocity components and bottom friction are defined on the grid sides and all other variables are given at the grid center.

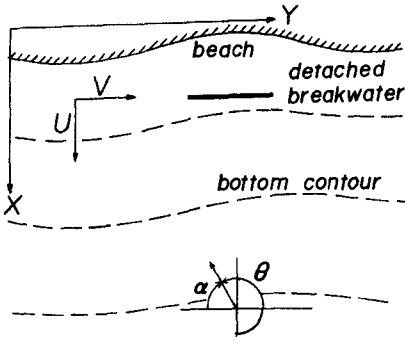


Fig. 1 Coordinate system used in nearshore current computation.

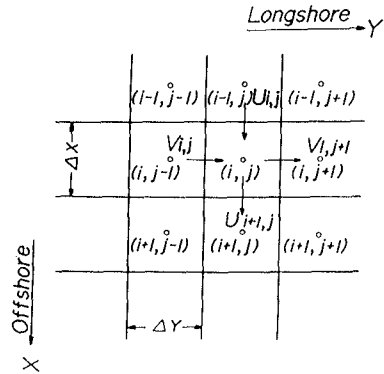


Fig. 2 Configurations of variables in finite difference model.

(3) Topographical change model

The two-dimensional continuity equation of sediment transport may be written as

$$-\frac{\partial h}{\partial t} + \frac{1}{(1-\lambda)} \left(\frac{\partial q_x}{\partial x} + \frac{\partial q_y}{\partial y} \right) = 0 \tag{10}$$

in which λ (0.3) is the bottom sediment porosity, and q_x and q_y are the local sediment transport rate components in x direction and in y direction respectively.

The Tsuchiya model (1982) is extensively applied to the evaluation of local sediment transport rate q in a two-dimensional flow field. The model was derived from the assumption that waves are responsible for the stirring up of bottom materials and that currents transport sediments in their direction. It can be expressed as

$$q = c_0 \frac{\rho}{\rho_d} \left(1 - \frac{\tau_c^*}{\tau^*} \right) D \sqrt{U^2 + V^2} \tag{11}$$

in which c_0 (0.02) is the average concentration of sediments, ρ_d/ρ (2.65) the specific weight of sediments, τ^* the Shields parameter and τ_c^* the value at the critical stage of sediment movement.

The finite difference method used in the numerical integration of eq. (10) is the same as that of eq. (6). In this case, local sediment transport rate components are estimated by redistributing the local sediment transport rate evaluated

at the grid center to the grid sides which define nearshore current components.

(4) Boundary condition and computational procedure

The initial condition and conditions for an offshore fixed boundary and an onshore moving boundary used in the model are the usual ones. In the longshore direction, the periodic boundary condition proposed by E. Noda (1974) is imposed on all the variables relevant to the computation. Moreover, no-flow condition is assumed at the structure boundary.

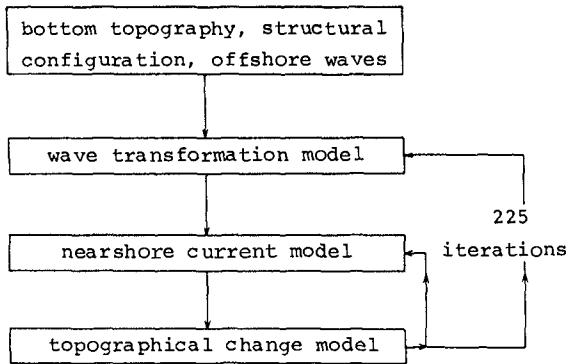


Fig. 3 Schematic diagram of computation flow.

The computer program starts with the determination of the spatial distribution of wave characteristics under the given conditions of offshore waves, bottom topography and structure configuration, and then nearshore current computation is carried out by using radiation stress estimated from the wave transformation model. A steady state solution of the nearshore current was obtained by 1260 iterations. Subsequently, alternating computation between the nearshore current and topographical modification was initiated. During the computation, the wave characteristics were recalculated every 225 iterations in order to take into account the effect of topographical change. The schematic diagram of computation flow is shown in Fig. 3.

3. EXPERIMENTAL VERIFICATION OF NEARSHORE CURRENT MODEL

The computation of the nearshore current pattern is compared with the Isobe experiment (1980) for the purpose of verifying the applicability of the present model. The experiment was conducted on a plane beach with the slope of $i = 0.05$ and

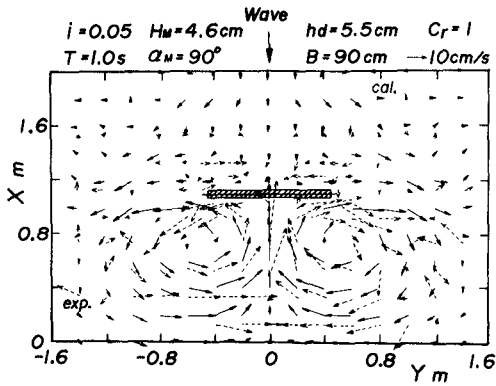


Fig. 4 Comparison of model computation with experiment for nearshore current pattern.

constant water depth of $h = 25.8$ cm in the offshore region. In the wave basin, an iron plate detached breakwater with the length of $B = 90$ cm was placed parallel to the shoreline at the water depth of $h_d = 5.5$ cm. The incident wave height, wave period and incident wave angle of waves used in the experiment were $H_M = 4.3$ cm, $T = 1$ s and $\alpha_M = 90^\circ$ respectively.

The comparison of the computed nearshore current pattern with the experiment is indicated in Fig. 4, in which C_r is the reflection coefficient of the breakwater. The overall characteristics of the current pattern, such as the formation of a pair of circulation currents with the opposite direction of rotation behind the breakwater, are in qualitative agreement with the experiment. But, the current pattern in the upside of the breakwater is slightly different from the experiment. Further testing is needed to verify the applicability of the present model.

4. NUMERICAL SIMULATION OF BOTTOM MODIFICATION

(1) Conditions used in model computation

As shown in Fig. 5, the configurations of coastal structures used in the model computation are from six cases; i) one detached breakwater placed parallel to the shoreline, ii) two detached breakwaters placed parallel to the shoreline, iii) one groin placed perpendicular to the shoreline, iv) two groins placed perpendicular to the shoreline, v) one groin placed oblique to the shoreline, and vi) two groins placed oblique to the shoreline.

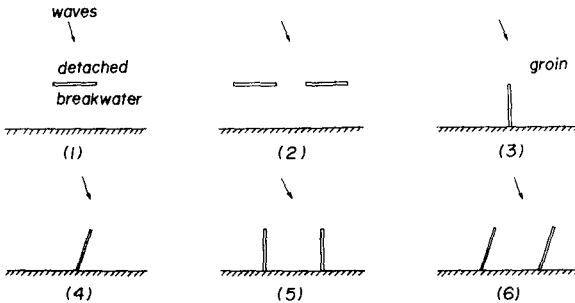


Fig. 5 Configuration of coastal structure used in computation.

The nearshore current pattern and change of the bottom topography are computed after 1 to 3 hours of constant wave action. The initial topography is taken as a plane beach with constant slope, although the present model is applicable to arbitrary bottom topography. The study area is divided into 15 points in the offshore x direction and 54 points in the longshore y direction with the grid distance of $\Delta x = \Delta y = 10$ m. The maximum water depth is $h_{max} = 4$ m and the time step used in the finite difference model is $\Delta t = 1$ s. The fixed conditions in the computation are the incident wave height ($H_M = 1$ m), wave period ($T = 3.5$ s) and beach slope ($i = 0.04$). The variable conditions are the incident wave angle (α_M), water depth of the structures (h_d or h_g), reflection coefficient of the structures (C_r), action time of waves (t), number of structures (1 or 2), length of the structures (B), distance between the structures (D_d or D_g) and the angle of structures to the shoreline (β_H).

The effects of these parameters on current pattern and bottom modification are investigated by comparison with the computed results for the standard condition, but only some of the examples are presented in this paper.

(2) Topographical change caused by detached breakwaters

Fig. 6 is the nearshore current pattern and the resulting topographical change after 1 hour of wave action for the standard conditions in the case of a detached breakwater. A large circulation current with clockwise rotation is formed on the downwave side behind the breakwater. But, a small circulation current found on the upwave side behind the breakwater before the beginning of topographical change computation disappears with the progress of bottom modification. Contourlines in the left side region behind the breakwater advance and bottom topography reveals the tendency of

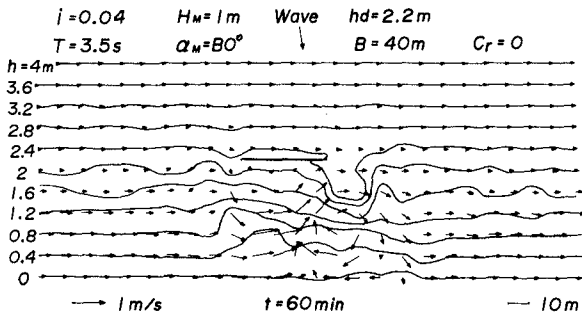


Fig. 6 Topographical change caused by a detached breakwater.

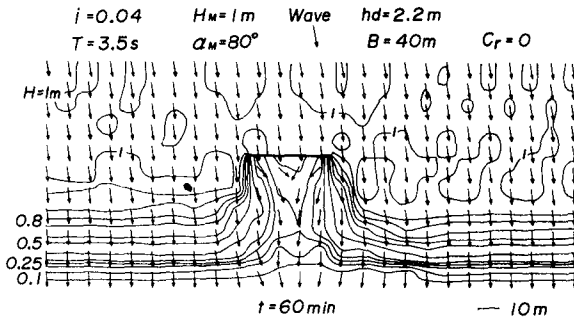


Fig. 7 Spatial distribution of wave height and wave direction in the case of a detached breakwater.

accretion in this area. On the other hand, contourlines in the area close to the right side of the breakwater retreat, and this results in the tendency of marked erosion in the region. However, the present model does not adequately produce the shoreline change, because swash transport of sediments is not included.

Fig. 7 is the spatial distribution of wave height and wave direction. Wave height decreases in the surf zone and in the shadow zone of the breakwater because of wave breaking and wave diffraction and in the offshore zone, it increases and decreases in space through the effect of diffracted waves.

Fig. 8 indicates the results after 3 hours of wave action. Meandering of the longshore currents is amplified with the progress of topographical modification. Accreting tendency on the left side reduces with the passage of time and the topographical change of the sea bottom approaches a state of

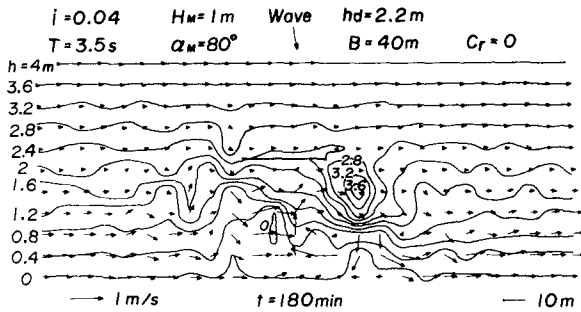


Fig. 8 Effect of action time of waves on topographical change in the case of a detached breakwater.

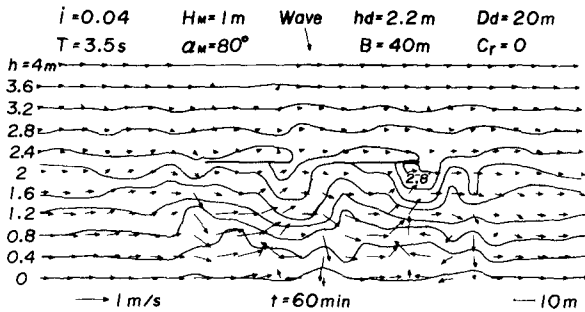


Fig. 9 Topographical change caused by two detached breakwater.

equilibrium. On the contrary, the eroding tendency on the right side continues and a scoured hole and the local advance of the shoreline are observed.

The results in the case of two detached breakwaters are given in Fig. 9. On the leeside of each breakwater, circulation currents are formed respectively, but their shapes are different from each other because of the effect of mutual interference between the two breakwaters. When the distance between the two breakwaters is longer, the interference effect becomes weaker and the circulation currents take a more similar shape. The feature of bottom modification is a similar situation. Contourlines behind each breakwater reveal slightly different changes. For instance, the scoured hole in the vicinity of the right edge of the right breakwater is deeper than the one on the right edge of the left breakwater.

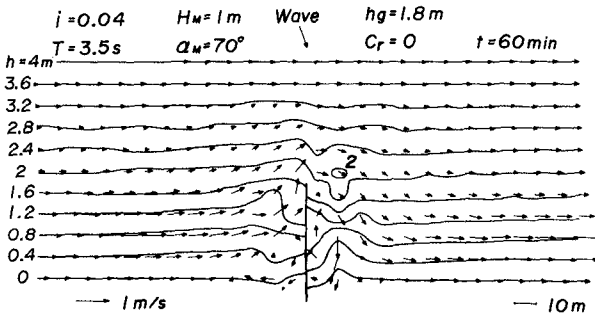


Fig. 10 Topographical change caused by a perpendicular groin.

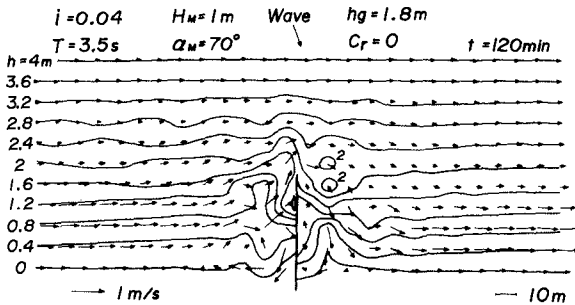


Fig. 11 Effect of action time of waves on topographical change in the case of a perpendicular groin.

(3) Topographical change caused by perpendicular groins

This section describes the bottom modification caused by groins placed perpendicular to the shoreline. Fig. 10 is the current pattern and bottom topography after 1 hour of wave action. In addition to the predominant longshore current moving around the groin tip, a small circulation current and a larger one are found in the frontal region of the groin and in the sheltered region respectively. The former current with the progress of topographical change. As a general feature of bottom modification, contourlines outside the surf zone advance on the left side of the groin and retreat on the right side. The contrary tendency is observed in the surf zone.

After 2 hours of wave action, the variation of nearshore current and bottom topography grows more and more as given

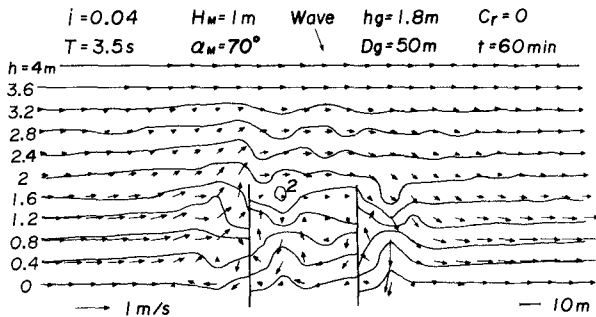


Fig. 12 Topographical change caused by two perpendicular groins.

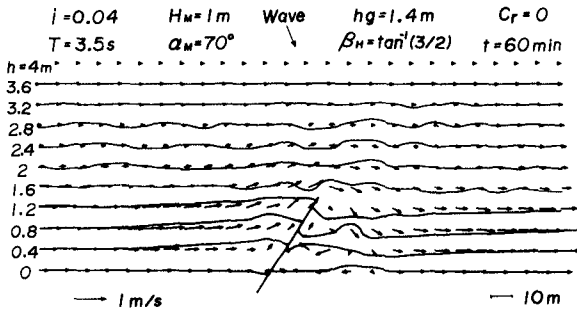


Fig. 13 Topographical change caused by an oblique groin.

in Fig. 11. As a result, we can see the overturning of contourlines in the vicinity of the groin tip.

The results computed for two perpendicular groins are plotted in Fig. 12. Four circulation currents are formed on both sides of the groins, but the corresponding circulation currents are different from each other in their shape and magnitude because of the mutual interference effect between the two groins. This current characteristics produce slightly different pattern of contourline change in the corresponding region of each groin, compared to the case of one perpendicular groin.

(4) Topographical change caused by oblique groins

Fig. 13 is the current pattern and contourline plots of modified bottom topography in the case of an oblique groin.

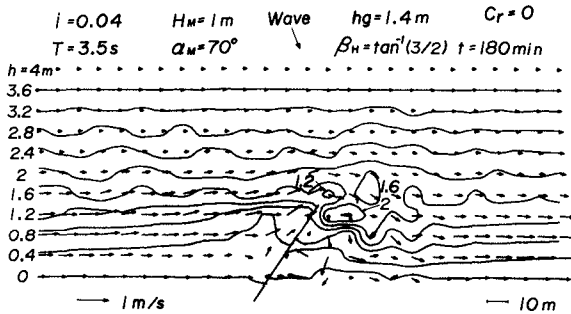


Fig. 14 Effect of action time of waves on topographical change in the case of an oblique groin.

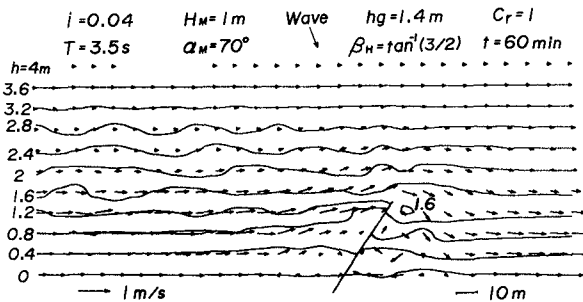


Fig. 15 Effect of wave reflection on topographical change in the case of an oblique groin (1).

The predominant longshore current passing around the groin and a clockwise circulation current in the sheltered region of the groin are observed as the case of a perpendicular groin, but a small circulation current in the upwave region of the groin toe is no longer formed. Contourlines in the upwave region advance and contourlines in the vicinity of the groin tip retreat, similar to those produced by a perpendicular groin. The difference is that the time for variation of bottom topography becomes slower compared to the case of a perpendicular groin.

After 3 hours of wave action, the current pattern and bottom topography are modified as shown in Fig. 14. The tendency mentioned above is promoted with the passage of wave action time, and isolated bars and locally-scoured holes are formed in the vicinity of the groin tip.

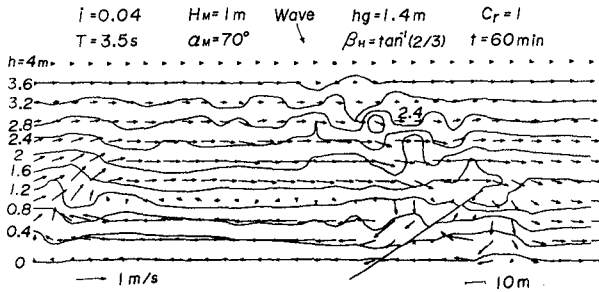


Fig. 16 Effect of wave reflection on topographical change in the case of an oblique groin (2).

Fig. 15 shows the effect of waves reflected from the groin, in the case where reflection coefficient is taken as 1. A small circulation current is formed at the toe of the groin on the upwave side by the influence of reflected waves. However, the overall characteristics of current pattern and bottom topography are not so different from Fig. 13, although the undulation of contourlines in the upwave region becomes greater by the influence of diffracted waves associated with reflected waves. This is because the region of reflected waves is confined in a smaller area for the present configuration of a groin.

In the case where the region of reflected waves is larger, the current pattern and bottom topography are drastically altered in the upwave region, as illustrated in Fig. 16. A clockwise circulation current with a large scale is formed in the upwave region and remarkable modifications of bottom topography take place.

Fig. 17 and Fig. 18 are the results computed after 1 to 3 hours of wave action in the case of two oblique groins. We can see the current pattern with the predominant longshore current going around the oblique groins and a circulation current with a slightly different scale formed behind each groin, as in the case of two perpendicular groins. The difference of the circulation current pattern was brought about by the mutual interference between the two groins and this affects the topographical change of the sea bottom in the area enclosed by the two groins. As a general feature, it can be said that the topographical change in this area is slower compared to that in the other area. Moreover, the progress of bottom modification tends to give rise to the reinforcement of nearshore current velocity and the greater variation of its direction in space at most sites investigated.

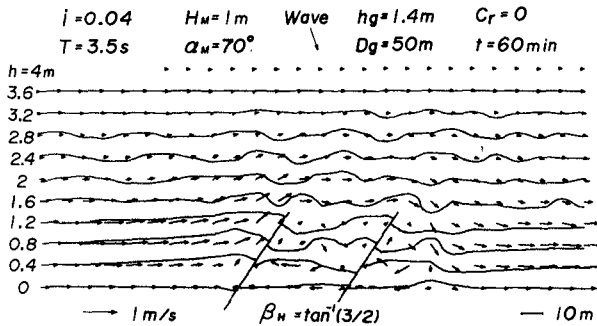


Fig. 17 Topographical change caused by two oblique groins.

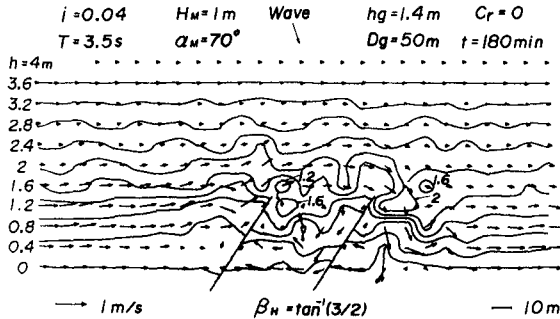


Fig. 18 Effect of action time of waves on topographical change in the case of two oblique groins.

5. CONCLUSIONS

The main conclusions of this study are summarized as follows.

- i) A numerical model for predicting the change in bottom topography caused by the presence of coastal structures was proposed by combining three submodels of wave transformation, nearshore current and topographical change of the sea bottom.
- ii) The model produces the general characteristics of erosion and deposition caused by the presence of coastal structures.
- iii) Drastic changes of current patterns and bottom topography occur when the reflected waves from coastal structures cover a large area.
- iv) Experimental verification of the computed results is needed to check the applicability of the proposed model.

and to improve the model.

6. ACKNOWLEDGEMENT

A part of this study was accomplished with the support of the Scientific Research Fund of the Ministry of Education, for which the authors express their appreciation.

7. REFERENCES

- Fleming, C.A. and J. N. Hunt (1976): Applications of a sediment transport model, Proc. of 15th Conf. on Coastal Engg., Vol. II, pp. 1184 - 1202.
- Gōda, Y. (1975): Deformation of irregular waves due to depth-controlled wave breaking, Rept. of Port and Harb. Res. Inst., Vol. 14, No. 3, pp. 57 - 106 (in Japanese).
- Isobe, M. (1980): Cooperative study on the dynamics in surf zone (II) - natural beach and breakwater-defensed coast -, Nearshore Environment Research Center, Rept. 10, pp. 130 - 145 (in Japanese).
- Longuet-Higgins, M.S. (1970): Longshore current generated by obliquely incident sea waves, Jour. of Geophys. Res., Vol. 75, No. 33, pp. 6778 - 6789.
- Nishimura, H. (1982): Numerical simulation of nearshore circulation, Proc. of 29th Japanese Conf. on Coastal Engg., pp. 333 - 337 (in Japanese).
- Noda, E.K. (1974): Wave-induced nearshore circulation, Jour. of Geophys. Res., Vol. 79, pp. 4097 - 4106.
- Tsuchiya, Y. (1982): The rate of longshore sediment transport and beach erosion control, Proc. of 18th Conf. on Coastal Engg., Vol. II, pp. 1326 - 1334.
- Yamaguchi, M., S. Ōtsu and Y. Nishioka (1981): Numerical simulation of three-dimensional beach change caused by a detached breakwater, Abstract of 36th Annual Meeting of JSCE, pp. 849 - 850 (in Japanese).
- Yamaguchi, M., Y. Nishioka and S. Ōtsu (1983a): Numerical simulation on the change of bottom topography by the presence of coastal structures, Memoirs of the Faculty of Engg., Ehime Univ., Vol. X, No. 2, pp. 275 - 283 (in Japanese).
- Yamaguchi, M. and Y. Nishioka (1983b): Computational method of three-dimensional beach change caused by detached breakwaters or groins, Proc. of 30th Japanese Conf. on Coastal Engg., pp. 239 - 243 (in Japanese).

Yamaguchi, M. and Y. Nishioka (1984): Numerical simulation on the change of bottom topography by the presence of coastal structures (2) - cases for two detached breakwaters or two jetties -, Memoirs of the Faculty of Engg., Ehime Univ., Vol. X, No. 3, pp. 399 - 406 (in Japanese).